Title
Feasibility of graphene CRLH metamaterial waveguides and leaky wave antennas

Journal
Journal of Applied Physics, 120(1)

ISSN
0021-8979

Authors
Chu, Derrick A
Hon, Philip WC
Itoh, Tatsuo
et al.

Publication Date
2016-07-07

DOI
10.1063/1.4955138

Peer reviewed

Feasibility of graphene CRLH metamaterial waveguides and leaky wave antennas

Derrick A. Chu,[1] Philip W. C. Hon,[1,2] Tatsuo Itoh,[1] and Benjamin S. Williams[1,3,a)]

[1)] *Department of Electrical Engineering, University of California, Los Angeles, CA 90095 USA.*

[2)] *NG NEXT Nanophotonics and Plasmonics Laboratory, Northrop Grumman Aerospace Systems, Redondo Beach, CA 90278 USA.*

[3)] *California NanoSystems Institute (CNSI), University of California, Los Angeles, CA 90095 USA.*

(Dated: 14 June 2016)

The feasibility of composite right/left-handed (CRLH) metamaterial waveguides based upon graphene plasmons is demonstrated via numerical simulation. Designs are presented that operate in the terahertz frequency range along with their various dimensions. Dispersion relations, radiative and free-carrier losses, and free-carrier based tunability are characterized. Finally, the radiative characteristics are evaluated, along with its feasibility for use as a leaky-wave antenna. While CRLH waveguides are feasible in the terahertz range, their ultimate utility will require precise nanofabrication, and excellent quality graphene to mitigate free-carrier losses.

PACS numbers: 81.05.Xj

Keywords: Graphene, CRLH, Metamaterial, Plasmonics, Terahertz

[a)] Electronic mail: bswilliams@ucla.edu

I. INTRODUCTION

Graphene shows considerable promise as an optical material in the terahertz and mid-infrared frequency ranges as a result of the strong optical response associated with intraband conduction of Dirac fermions. Two-dimensional plasmons in single and multi-layer graphene structures have been extensively described theoretically and via numerical simulations.[1–5] Furthermore, direct evidence of their existence has been shown in the THz and mid-IR using near-field probe techniques,[6–9] as well using infrared absorption spectroscopy in patterned structures (micro- and nano-ribbons, discs, dipoles, etc.) to excite dipolar modes associated with standing-wave plasmons.[10–12] For sheet carrier concentrations of $\sim 10^{12} - 10^{13}$ cm^{-2} THz resonances can be achieved for structures with widths of several microns;[10,11] if the sizes are reduced to tens of nanometers, resonances in the 3–12 μm range can be obtained.[12–14] By leveraging these effects graphene has been demonstrated as a THz modulator,[15–17] and has been proposed for strong light-matter coupling[3,12] as well as for resonant and leaky-wave antennas.[18–21]

In this paper we explore the feasibility of graphene for composite right/left-handed (CRLH) metamaterial waveguides in the terahertz and far-IR frequency range (1–15 THz). The CRLH metamaterial concept is most easily understood using transmission-line theory. A conventional (right-handed) transmission-line has a series inductance (L_R) and a shunt capacitance (C_R); by loading the line with distributed series capacitance (C_L) and shunt inductance (L_L), the line becomes highly dispersive and exhibits backward wave (left-handed) propagation.[22–24] The dispersion relation of the angular frequency ω vs. the propagation constant β is shown for a typical CRLH line in Fig. 1. A stopband is evident at $\beta = 0$, where the band edge frequencies are given by the shunt resonance $\omega_{sh} = (L_L C_R)^{-\frac{1}{2}}$ and series resonance $\omega_{se} = (L_R C_L)^{-\frac{1}{2}}$. If the line is properly designed, these resonance frequencies can be made equal so that the stopband closes; this is known as the balanced condition. A balanced CRLH line is particularly useful for traveling wave devices since all modes exhibit non-zero group velocity, and the characteristic impedance of the line is independent of frequency. One- and two-dimensional metamaterials have been widely explored in the microwave frequency range, and have been used to demonstrate a variety of guided-wave devices (e.g., multi-band and enhanced bandwidth components, power combiners/splitters, compact resonators, phase shifters, and phased array feed lines), as well as radiating devices

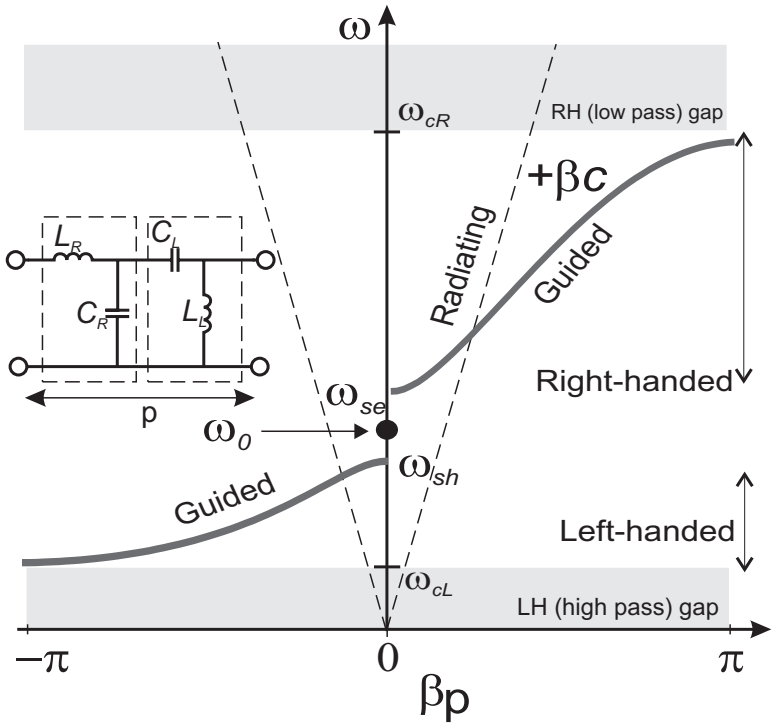

FIG. 1. CRLH dispersion relationship which exhibits both right- and left-handed characteristics. A stopband exists between ω_{sh} and ω_{se} - the shunt and series resonance frequencies respectively. The inset shows the characteristic CRLH transmission line unit cell, which contains series inductance L_R, shunt capacitance C_R, series capacitance C_L, and shunt inductance L_L.

(e.g., 1D and 2D resonant and leaky-wave antennas).[23,25] More recently CRLH metamaterial waveguides and metasurfaces have been demonstrated in the THz frequency range, both for passive waveguides, as well as in active devices integrated with THz quantum-cascade laser gain material.[26,27]

II. DESIGN

A. Conductivity model and graphene plasmons

We begin by considering the propagation of plasmons by infinite, unpatterned graphene sheets on a dielectric half-space. If coupling with free-space propagating electromagnetic waves is neglected, graphene plasmons are described by a dispersion relation for the in-

plane wavenumber q:

$$q = \frac{i\,(\varepsilon_1 + \varepsilon_2)\,\omega}{\sigma(\omega)}, \tag{1}$$

where ε_1 and ε_2 are the permittivities of the two dielectric regions, and $\sigma(\omega)$ is the ac sheet conductivity of the graphene. Throughout this paper we model the graphene conductivity using the Drude model as given by:[28]

$$\sigma_{2D}(\omega) = \frac{e^2 E_F}{\pi\hbar^2}\frac{\tau}{1 - i\omega\tau}, \tag{2}$$

where E_F is the Fermi level, $v_F = 10^6$ m/s is the Fermi velocity, e is the fundamental charge, $\hbar$ is the reduced Planck constant, and τ is the Drude momentum relaxation time. The Fermi level is related to the sheet carrier density n by

$$E_F = \hbar v_F \sqrt{\pi |n|}. \tag{3}$$

Inserting the Drude conductivity into (1) gives the dispersion relation:

$$q(\omega) = \frac{\pi\hbar^2(\epsilon_1 + \epsilon_2)}{e^2 E_F}(1 + \frac{i}{\tau\omega})\omega^2, \tag{4}$$

which exhibits the characteristic $\omega \propto q^{1/2}$ behavior associated with 2D plasmons and the $\omega \propto n^{1/4}$ behavior associated with a Dirac bandstructure.[2]

It has been shown that the Drude model for conductivity does an excellent job of capturing the essential behavior of graphene plasmons, particularly when the wavenumber q is modest compared to the Fermi wavenumber ($q \ll E_F/\hbar v_F$),[29] and at sufficiently low temperatures such that $k_B T \ll E_F$. Both conditions are well satisfied for the doping levels of graphene considered here where $n \geq 10^{12}$ cm^{-2} ($E_F \geq 0.13$ eV). Since we will consider plasmons with frequencies of at most 15 THz ($\hbar\omega \sim 62$ meV)), interband transitions will be forbidden since $\hbar\omega \ll 2E_F$. More accurate conductivity expressions that include interband transitions and comparisons with random-phase-approximation (RPA) based models are given in Ref. 29; treatments of nonlocal conductivity (i.e. spatial dispersion) are given in Ref. 30 and 31. It has been shown that classical local models for the conductivity are generally accurate for graphene nanostructures larger than ∼20 nm.[32] Our confidence in using the local Drude conductivity is further bolstered by reports which show that even for 60 nm wide graphene nanoribbons, use of a nonlocal conductivity model (where conductivity $\sigma(\omega, q)$ is a function of both frequency and wavenumber) only shifts resonances by 5% or less for our considered carrier concentrations.[33] For larger nanostructures at lower frequencies, the shifts are smaller,

since the in-plane wavenumbers q involved are smaller. As a final check, we have performed a post-computational analysis on our simulation results by using Fourier analysis to extract the spectral power of the current density distribution. For the frequencies and dimensions considered here, we confirmed that 95% or more of the spectral power is at wavenumbers sufficiently small that corrections due to spatial dispersion are a few percent or less.[30,31]

B. Design of CRLH waveguide

Since CRLH metamaterials are typically described using transmission-line (TL) models, it is useful to begin our discussion by describing the fundamental lateral plasmon mode ($m = 0$) on a microribbon of width w using a transmission line (TL) model (e.g. as in Refs. 31 and 34). This mode is schematically illustrated in Fig. 2(a) along with its dispersion relation. In the low-damping limit ($\omega\tau \gg 1$), the kinetic inductance of the electrons dominates the graphene impedance; this can be represented by an equivalent series inductor L_R in the circuit diagram in Fig. 1. The fringing E-field longitudinally couples charges along the graphene ribbon and plays the role of the shunt capacitor C_R. Effective values for these circuit elements are given in the Appendix.

In order to realize a CRLH line, a shunt inductance L_L and a series capacitance C_L must be added. It is straightforward to create a distributed series capacitance by introducing repeated gaps of size a and period p along the graphene microribbon. This adds a high-pass characteristic to the dispersion relation for the $m = 0$ mode, with a cutoff frequency equal to the series resonance ω_{se} (see Fig. 2(b)).

In microstrip implementations, the shunt inductance L_L is typically achieved using a stub and/or a via to the ground plane. At THz frequencies such techniques are often lossy and difficult to fabricate; furthermore they are incompatible with the geometry of a single graphene microribbon. However, an effective shunt inductance arises naturally if we consider propagation of the first higher-order lateral mode (labeled $m = 1$) of the microribbon (also known as an edge mode), which is associated with transverse conduction currents. This can be modeled by two transmission lines in parallel, coupled together by an inductance $2L_L$ (see Fig. 2(c)). The effective shunt resonant frequency ω_{sh} is given by the cutoff frequency for this higher order mode, which occurs when the the width w is approximately equal to one half of the plasmon wavelength, i.e. $q(\omega_{sh}) \approx \pi/w$. This approach to obtaining L_L has

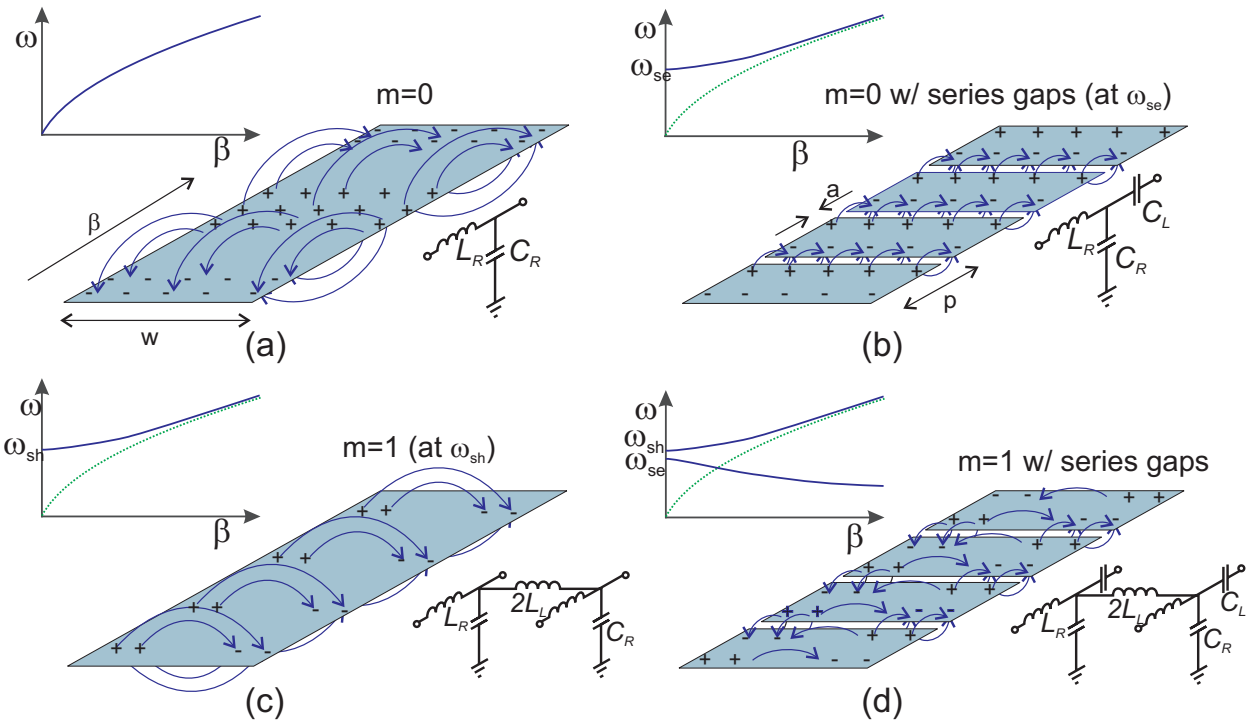

FIG. 2. Conceptual design progression for CRLH graphene plasmonic waveguide along with their associated circuit models (for one unit cell) and dispersion relations. (a), (b) show the fundamental $m = 0$ even mode with and without series gaps. (c), (d) show the higher order $m = 1$ odd mode with and without series gaps. The latter case shown in (d) exhibits CRLH behavior and is the basis for the designs presented here.

been used for passive and active THz microstrip-type waveguides.[26,27,35]

When gaps are introduced, the dispersion of the $m = 1$ mode takes on a CRLH character, with both right-handed and left-handed propagating characteristics. The double transmission line model is shown in Fig. 2(d). When this line is excited in its odd mode, the central symmetry plane acts as a virtual ground, so that each branch is equivalent to the circuit in Fig. 1. With proper design, one can obtain the condition $\omega_{se} = \omega_{sh}$, and we say the structure is "balanced"; the stopband closes and propagating waves exist with non-zero group velocity even at $\beta = 0$.

III. RESULTS: DISPERSION CHARACTERISTICS

A. Simulation Methodology

Numerical simulations were performed using a commercial finite element full-wave electromagnetic solver (Ansys HFSS). The eigenfrequency solver was applied to a single unit cell of length p with periodic Floquet-Bloch boundary conditions in the axial direction for a fixed propagation constant β; this was used to extract the complex eigenfrequency $\omega = \omega' + i\omega''$. This procedure allowed the retrieval of the dispersion relationships $\omega'(\beta)$.

The graphene is modeled as a 2D impedance boundary condition of $Z_s = \sigma(\omega')^{-1}$ at the dielectric halfspace interface, where the conductivity σ is taken from Eq. (2).[36] The simulation space consisists of a cylindrical "airbox" of 15 μm radius surrounding the graphene microribbon. The upper semi-cylinder has permittivity ε_1 (assumed to be vacuum throughout), and the lower semi-cylinder has permittivity ε_2 which represents a semi-infinite substrate. For radiating modes, it is important to suppress reflections at the transverse airbox boundaries; this is accomplished by using a layered impedance boundary condition. Various airbox sizes were considered to verify that their dimensions did not affect the complex eigenfrequency solution.

Since the conductivity of graphene is dependent on frequency, an iterative approach was used to achieve a self-consistent solution. The algorithm is as follows: first, for a given value of β an inital radian frequency ω_0 is guessed using the lumped element circuit model; this value is used to calculate $\sigma(\omega_0)$ for graphene which is input into the simulation, and the complex eigenfrequency ω_i is solved numerically for each i-th iteration. Second, the conductivity $\sigma(\omega_i')$ is used to re-solve for the eigenfrequency ω_{i+1} The process is iterated until the real part of the complex eigenfrequency converges within 20 GHz. As verification, this method is seen to accurately reproduce the analytic dispersion relation for an unpatterned graphene microribbon in its fundamental $m = 0$ mode in Fig. 3.

The imaginary part of the eigenfrequency gives information both about Drude loss and radiative loss (for modes within the light line ($\beta < n\omega/c$)). The modal quality factor Q is obtained from the complex eigenfrequency according to $Q = \omega'/2\omega''$, and with knowledge of the group velocity $v_g = d\omega'/d\beta$ of the mode, the power loss coefficient per unit length is given by $\alpha = \omega'/Qv_g$.

However, a complication arises if the finite element eigenfrequency solver is used to directly extract the Drude losses, because the graphene impedance is treated as frequency independent during any given iteration. Essentially the imaginary part of the impedance is not allowed to vary with frequency during the eigenfrequency solution process (equivalent to finding a root in complex frequency space). This results in the eigenfrequency solver underestimating the Drude contribution to the losses by as much as a factor of two (depending upon the value of β). For example, for the $m = 0$ guided mode, the HFSS solver calculates $Q = \omega\tau/2$, instead of the expected $Q = \omega\tau$ that can be calculated analytically from Eq. (4). This issue is addressed in detail in Sec. IV A via a hybrid method, where only the radiative losses are extracted numerically, and an analytic expression is used for the Drude losses based upon a transmission line model.

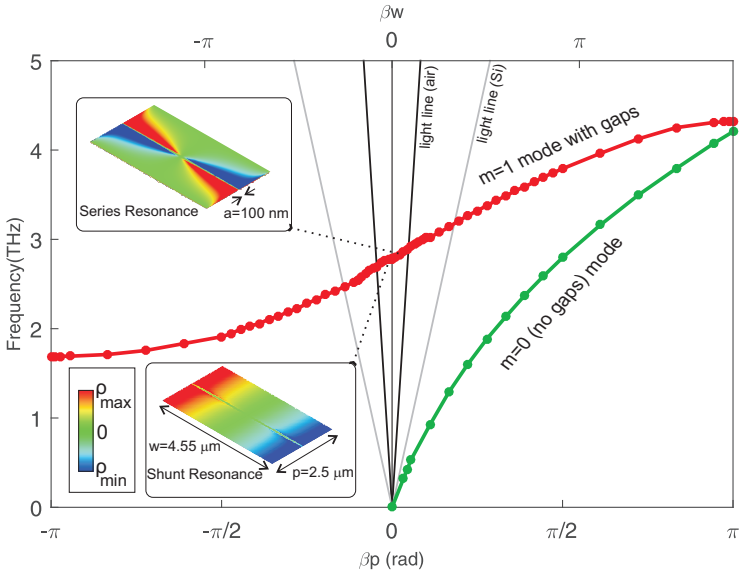

FIG. 3. Simulated dispersion relationship for Design A CRLH structure ($m = 1$ with series gaps) with a center frequency of 2.8 THz (red) and dimensions shown. Also shown is the dispersion for the $m = 0$ plasmonic mode on a graphene microribbon of identical width (green). Shown in the insets are plots of the graphene charge density ρ at the shunt and series resonance. Light lines ($\omega = c\beta/n$) for vacuum ($n = 1$) and silicon ($n = 3.41$) are also plotted in black and gray, respectively.

B. Design of a Baseline CRLH structure

An exemplar CRLH waveguide was designed to operate with a center frequency of 2.8 THz, with dimensions as follows: unit cell length $p = 2.5$ μm, capacitive gap size $a = 100$ nm, and microribbon width $w = 4.55$ μm. Design proceeds as follows. For a given carrier density, the width w of the microribbon is chosen first to set ω_{sh} to the frequency of choice. The circuit model is used to give a coarse estimate (see Appendix); the value is then refined using a 2D full-wave simulation for a finite width ribbon. Then gaps are added to the design, with an initial guess for the period p and gap size a again provided by the circuit model. Then the dimensions are fine tuned using full-wave simulations so that the CRLH structure is nearly balanced (i.e. $\omega_{sh} = \omega_{se}$). For this baseline design, which we will refer to as "Design A," the carrier density was taken as $n = 3 \times 10^{13}$ cm^{-2} ($E_F = 0.64$ eV), a value which is readily experimentally achievable. We also assumed that the graphene structure was at the interface of a dielectric half-space between vacuum and a lossless silicon substrate ($\varepsilon_r = 11.6$). This was chosen somewhat arbitrarily, and our results should be understood to be applicable to a variety of dielectric substrates (i.e. SiO_2, BN, etc.), provided the appropriate modifications are made to the dimensions, plasmon damping rates, and substrate dielectric and free-carrier losses. Similarly, we have neglected any coupling with optical phonon *Reststrahlen* bands in the substrates;[12] such coupling is negligible at THz frequencies, but is important in the mid-IR (i.e. $\lambda \sim 10\,\mu$m for SiO_2 and BN). Unless otherwise specified, momentum relaxation time was set to be $\tau = 1$ ps. However, simulations showed that provided $\omega\tau > 1$, the dispersion relation is not sensitive to the particular value of τ. The simulated dispersion relation is presented in Fig. 3, and exhibits the characteristics shown in Fig. 1. Left-handed propagation is exhibited between 1.8–2.8 THz. The structure is nearly balanced, however, if closely examined, there is a slight ~20 GHz gap that remains at $\beta = 0$. At this point distinct series and shunt resonance modes can be observed, and their charge densities are shown in the inset of Fig. 3. However, when one considers non-zero values of β, the propagating modes are hybrids of these two basis states. For comparison, also shown in this figure is the dispersion of the fundamental $m = 0$ mode for a ribbon without gaps, which exhibits the characteristic $\omega \propto \beta^{1/2}$ behavior. As expected, the shunt resonance frequency occurs close to the half-wavelength condition (i.e. $\beta(\omega_{sh})w \approx 0.9\pi$ for the $m = 0$ mode). The residual 20 GHz gap is likely due to the imbalances in radiative losses

associated with the shunt and series branches of the transmission line.[37,38]

Several factors drive the choice of p. While ideally p should be as small as possible to obey the metamaterial homogenization condition, in practice as long as the period satisfies the condition $p < (2\pi/q)/2$ no higher order Bragg scattering will contribute to propagation. The finite-sized unit cell also gives rise to a high-pass filtering effect, where the series capacitance and shunt inductance behave as a high pass filter with a cutoff of $\omega_{cL} = 1/2\sqrt{L_L C_L}$, which is seen to be approximately 1.8 THz in this design. Reducing the unit cell size p results in a larger value of L_L and C_L (required to keep ω_{sh} and ω_{se} constant) which reduces the cutoff frequency. This can be used to engineer the group velocity and leaky-wave bandwidth of the CRLH waveguide. From a practical standpoint, reducing the unit cell is challenging, since the series capacitance has an only a logarithmic dependence on the gap size a. For example, our simulations showed that modifying Design A by reducing the period from 2.5 μm to 1 μm requires reducing the gap size from 100 nm to 1.3 nm to maintain the balanced condition.

C. Carrier density tunability

One of the attractive features of graphene is the ability to tune the plasmon dispersion via electrostatic gating, chemical doping, or optical pumping. This property can be exploited to tune CRLH waveguides while approximately maintaining their balanced character. Simulated dispersion relations for various concentrations for our Design A structure are shown in Fig. 4. Based on the graphene dispersion relationship presented in (4) we expect a fourth root scaling of frequency with carrier density (i.e. $\omega \propto n^{1/4}$). Indeed this is observed where two orders of magnitude change in carrier density shifts the center frequency by approximately a factor of three. This will prevent tuning of a single structure into different frequency ranges — say from the THz to the mid-IR. However, this tuning is more than sufficient to tune a graphene structure across the leaky-wave bandwidth (i.e. hundreds of GHz) for a beam-scanning or phase shifter application. For example, a phase shift of π radians can be obtained across a single unit cell by changing the carrier density by a factor of ten. Fig. 4 shows that the balanced condition is *approximately* preserved even as the carrier density is changed. Indeed, this is predicted by the analytic transmission-line treatment given in the Appendix for which only geometric parameters determine the balanced condition. However, it is seen that slight unbalancing occurs as the carrier density is tuned; whether this is within

acceptable limits will depend upon the application.

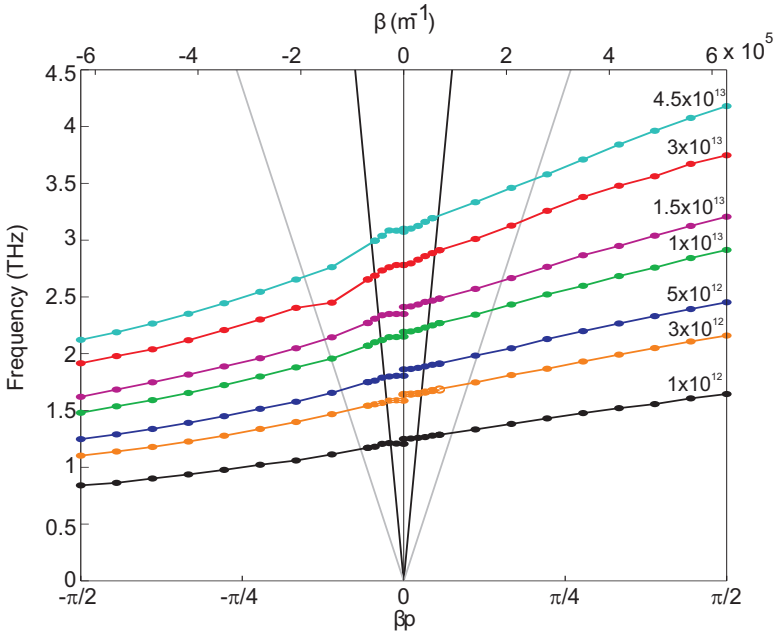

FIG. 4. Dispersion relationships for Design A for various graphene carrier densities labeled in units cm^{-2}.

D. Frequency scalability

Table I presents the dimensions of several CRLH waveguides designed for center frequencies of 2.8 THz, 5 THz, and 12 THz – labeled designs A, B, and C respectively. Dispersion relations for Design A, B, and C are plotted in Fig. 5, along with transmission line model fits obtained using the model and parameters given in the Appendix. It is seen that excellent agreement is obtained, although the use of several adjustable parameters is required to properly fit the numerical results. Unfortunately, the $q^{1/2}$ nature of graphene dispersion means that the width w must be reduced quadratically to achieve linear increases in frequency. This is seen in our designs, where frequency is scaled up by a factor of 4.2 from 2.8 THz (Design A) to 12 THz (Design C), requiring the width w to be downscaled by a factor of 17, and period p by a factor of 12.5. The gap size a shrinks only by a factor of 5 from 100 nm to 19 nm; the ability to fabricate increasingly small gaps will no doubt be a limiting factor in any attempt to realize mid-IR CRLH designs at 20-100 THz. We do not present such higher frequency designs here since the small dimensions result in increasingly large corrections on

the graphene conductivity model due to spatial dispersion (i.e. non-local conductivity).[30,31] Such effects are not readily incorporated into the finite-element eigenfrequency simulations used here.

TABLE I. Dimensions of frequency scaled designs

Design	**Center frequency**	**Periodicity** p	**Width** w	**Gap** a
A	2.8 THz	2.5 μm	4.55 μm	100 nm
B	5 THz	0.8 μm	1.42 μm	40 nm
C	12 THz	0.2 μm	0.260 μm	19 nm

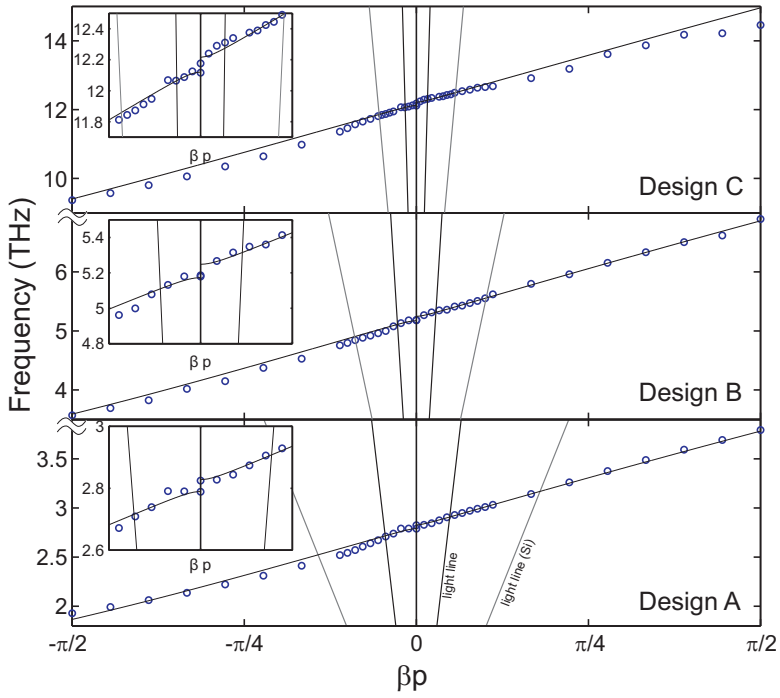

FIG. 5. Simulated dispersion relations for the frequency scaled designs in Table I (points), along with fits to transmission line model presented in Appendix. Insets are zoomed in views of dispersion near $\beta = 0$.

IV. RESULTS: RADIATIVE PROPERTIES

A. Radiative and Drude Losses

In principle, graphene holds the promise of high mobility and low plasmonic dissipation — however in practice the plasmon damping rates depend sensitively upon the graphene quality and substrate interactions. Furthermore, for modes within the light line, radiative losses must also be considered. In this section we consider both sources of loss, and the consequences for CRLH graphene waveguides.

Radiative loss is calculated using the same finite element eigenfrequency solver described previously in Sec. III A. However, as previously discussed, the eigenfrequency solver overestimates Drude losses. Therefore we implemented a hybrid method, where Drude losses are deliberately suppressed within the simulation by setting $\tau > 1$ ns. As a result, the numerically simulated quality factor contains only radiative losses, which we label Q_r. The effect of free-carrier loss is separately estimated assuming $\tau = 1$ ps using the analytic expression for the Drude quality factor that is derived in the Appendix (see (A.11)). The total quality factor is then given by $Q^{-1} = Q_r^{-1} + Q_D^{-1}$. Both the quality factor and power loss coefficient α are plotted for the three designs in Fig. 6.

Several trends are evident. First, the Drude losses for $\tau = 1$ ps are very large – for Design A at 2.8 THz ($\alpha_D \sim$1500 cm^{-1}), which leads to short attenuation lengths ($\alpha^{-1} \approx 6\ \mu$m). The radiative loss is of similar magnitude, which implies implies a radiative efficiency of 50% or better, but further reduces the propagation length. Second, there is a notable discontinuity of Q_r at $\beta = 0$. This is due to the fact the CRLH waveguide is not perfectly balanced so that at $\beta = 0$ a small 20 GHz gap remains; at this point the modes retain their distinctive series and shunt resonance character. Only the shunt resonance mode exhibits dipolar character and radiates strongly, whereas the series resonance mode is quadrupolar and is essentially a "dark" mode with a large Q_r (see Fig. 6(a)). Away from $\beta = 0$ the CRLH propagating mode is a hybrid of both series and shunt resonances, which radiates only via its shunt dipolar component. In fact, the presence of this residual 20 GHz gap is likely a consequence of the fact that only the shunt-mode radiates while the series-mode is dark; closing the gap entirely to achieve a perfect balanced condition would require the series mode to radiate also, as described in Refs. 37 and 38. For designs B and C at higher frequencies, the total

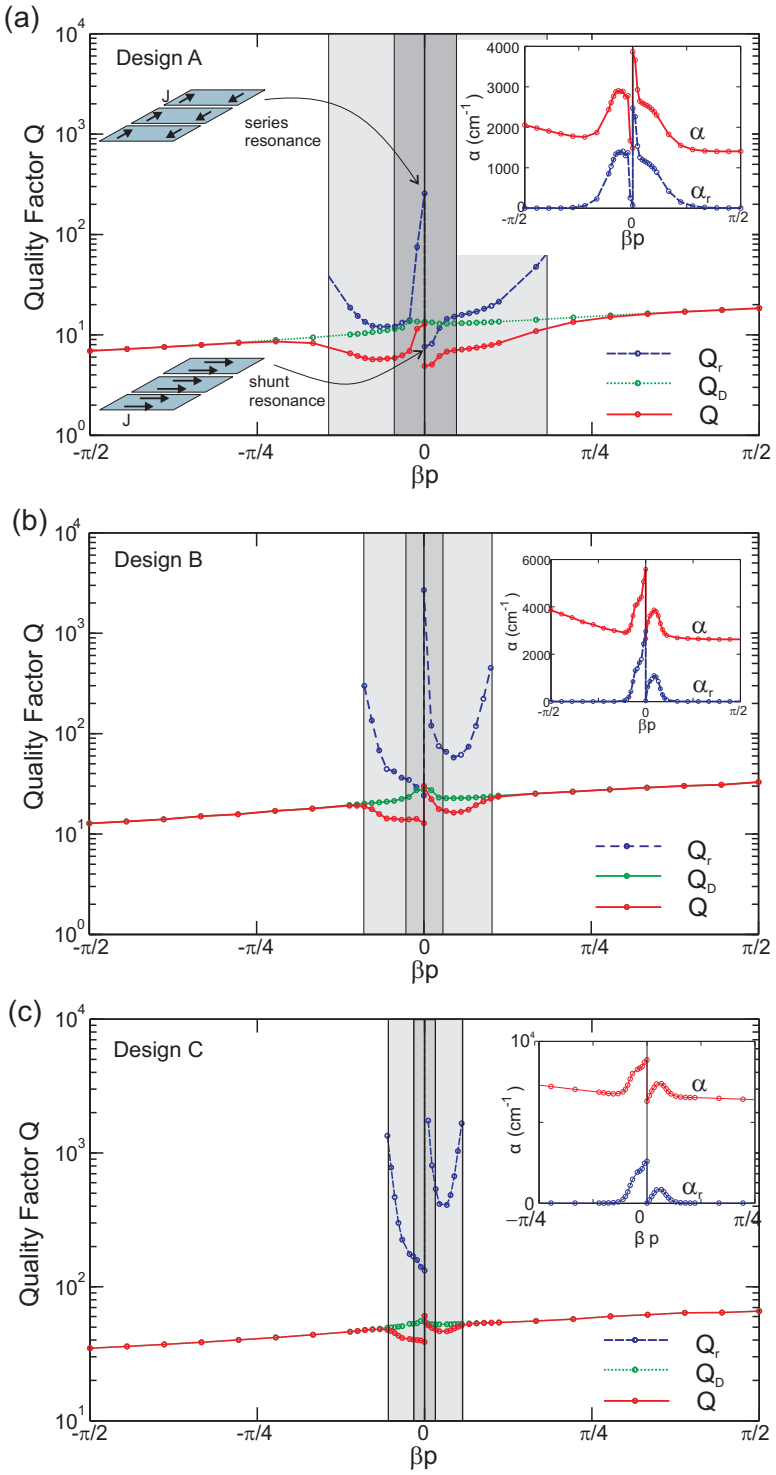

FIG. 6. Drude, radiative, and total quality factor assuming $\tau = 1$ ps for (a) Design A centered at 2.8 THz, (b) Design B centered at 5 THz, and (c) Design C centered at 12 THz. The shaded areas correspond to the air and silicon light cones. The insets plot the total and radiative power attenuation coefficient α. The cartoon in (a) illustrates the equivalent electric current sources for shunt and series resonances.

quality factor increases for two reasons. First, the Drude loss contribution scales as $Q_D \propto \omega$. Second, the radiative loss contribution also decreases for higher frequencies ($Q_r \propto \omega^2$) since the radiating dipole moment scales with the width w.

How realistic is τ=1 ps? Within the Drude model, the momentum relaxation time is related to the dc mobility μ according to $\tau = \mu E_F / e v_F^2$, so $\tau = 1\,\text{ps}$ corresponds to a mobility of 15,600 $\text{cm}^2/\text{V}\cdot\text{s}$ for $n = 3 \times 10^{13}\,\text{cm}^{-2}$. Dc mobilities greater than 100,000 $\text{cm}^2/\text{V}\cdot\text{s}$ have been observed at low temperature in suspended graphene,[39] and graphene on hexagonal boron nitride (h-BN) underlayers have demonstrated $\mu \approx 60,000\,\text{cm}^2/\text{V}\cdot\text{s}$ (exfoliated sample) as well as 37,000 $\text{cm}^2/\text{V}\cdot\text{s}$ (CVD grown).[40,41] When fully encapsulated in h-BN, graphene was shown to have room temperature mobilities as high as 120,000 $\text{cm}^2/\text{V}\cdot\text{s}$ at densities of 5×10^{11} cm^{-2}, and 40,000 $\text{cm}^2/\text{V}\cdot\text{s}$ at $3 \times 10^{12}\,\text{cm}^{-2}$, values which correspond to effective Drude relaxation times of $\tau \sim 0.8 - 1\,\text{ps}$. Direct measurement of plasmon damping at room temperature at $\lambda \sim 10\,\mu\text{m}$ has shown $\tau \sim 200 - 300\,\text{fs}$ in graphene/h-BN structures with no dependence on carrier density.[8] In summary graphene with $\tau \sim 1\,\text{ps}$ and perhaps even higher is certainly within experimental reach; future improvements in material quality will only help in achieving reduced losses. Values of $\tau \sim 0.1\,\text{ps}$ are more typical of graphene on SiO_2 substrates; such material quality is not sufficient for plasmonic CRLH waveguide operation in the THz.

B. Beam Scanning

A balanced CRLH based graphene structure can be considered for a leaky-wave antenna because its ability to scan its main beam from backwards to broadside to forwards.[25,42] Leaky-wave antennas in graphene have been proposed via various schemes that use Bragg scattering from periodic perturbation, such as sinusoidal modulation of the nanoribbon width,[21] or backgating to create a periodic reactance.[18] This proposed CRLH leaky-wave antenna would differ in two significant ways. First, radiation occurs because the fundamental dispersion of the metamaterial waveguide is within the leaky-wave region – not due to Bragg scattering. As a result, CRLH structures can be balanced so that there is no (in theory) or negligibly small (in practice) stopband at $\beta = 0$, which enables propagating waves across the entire leaky-wave band. Second, the radiation of our CRLH structure is mediated through transverse dipolar currents along the graphene microribbon (i.e. through

the shunt inductor). Coupling in and out of the metamaterial waveguide thereby occurs via coupling with transverse-electric (TE) plane waves, rather than transverse-magnetic (TM) plane waves, as is typical for conventional surface plasmons.[27]

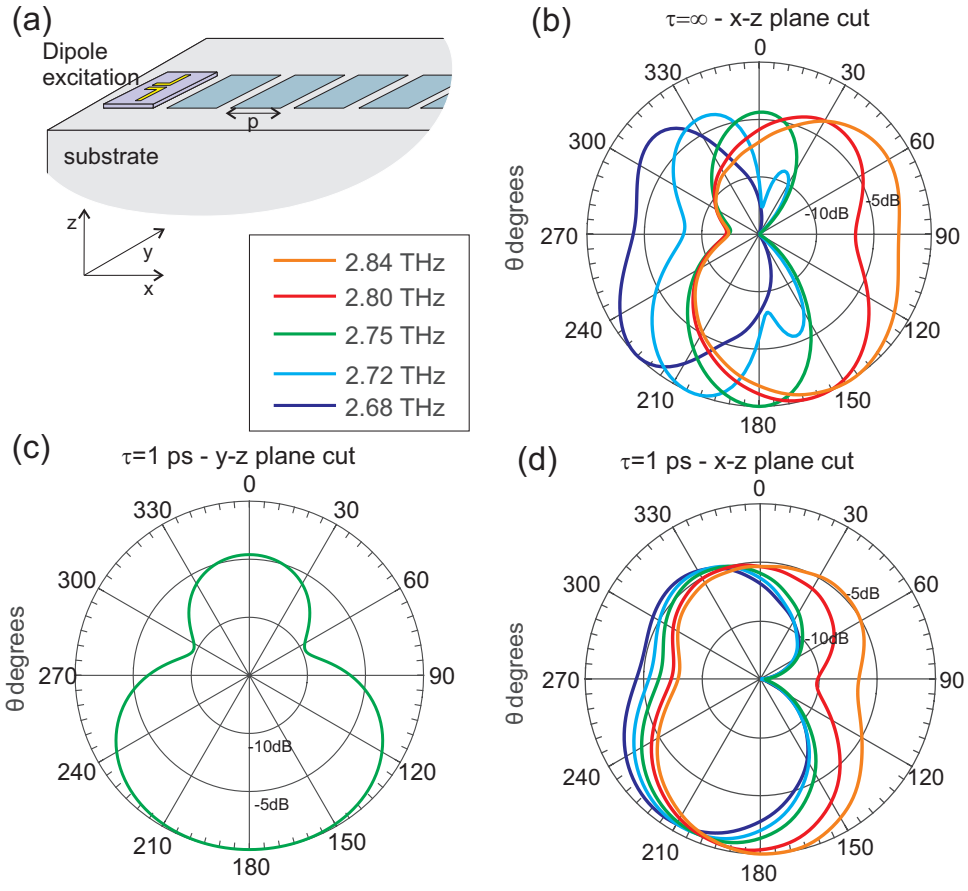

FIG. 7. (a) Schematic of near-field dipole antenna excitation scheme used for driven mode beam simulations. (b) Design A far-field intensity beam pattern in $x-z$ plane for five driving frequencies simulated with $\tau = \infty$. (c) Far-field intensity beam pattern in (c) $y-z$ plane at 2.75 THz and (d) $x-z$ plane simulated with $\tau = 1$ ps. All beams are normalized to unity peak intensity.

We study beam patterns from Design A using a driven 3D full-wave simulation, where a finite length ($300\,\mu$m) CRLH waveguide is excited as a LWA. We considered the Drude relaxation time as $\tau = 1\,$ps and $\tau = \infty$ (radiative losses only).

For the purposes of simulation, a near-field excitation is used to drive the CRLH mode, with a horizontal electrical dipole antenna placed $0.1\,\mu$m above the first unit cell as shown in Fig. 7(a). This is designed to excite the transverse current flow associated with the shunt resonance component of the CRLH mode. In practice, a CRLH LWA might be excited by

replacing the horizontal dipole with a photoconductive switch for narrowband THz generation via photomixing.[43] Alternately, the graphene CRLH structure might be excited using a microstrip-type waveguide — such as from a THz quantum-cascade laser — operating in its $m = 1$ higher-order mode.[26,35] Or, incident TE plane waves can be used to excite single or arrays of multiple CRLH waveguides.[27]

The CRLH structure primarily radiates into the silicon half-space with a beam that scans from backwards to forwards as the frequency is changed. In practice, radiation from the substrate could be out-coupled and directed using a silicon hemispherical lens as is common for THz photoconductive antennas. If Drude loss is neglected (as seen in Fig. 7(b)), scanning is observed in the x-z plane from 150 to 225 degrees. At 2.75 THz (near $\beta = 0$), the LWA radiates broadside with a fan-like beam. A typical beam pattern in the y-z plane is shown in Fig. 7(c). In the far-field, the electric field is predominately linearly polarized in the ϕ-direction (i.e. transverse to the LWA axis). This is consistent with our understanding of radiation originating from the transverse electric current dipoles associated with the shunt resonance component of the CRLH mode. The cross polarized component is smaller by 10 dB or more. When a Drude relaxation time of $\tau = 1\,\mathrm{ps}$ is used, the attenuation length is shorter, so the beam is broader, and scanning is much less pronounced, from 180 to 210 degrees (see Fig. 7(d)). This highlights the importance of high mobility graphene for leaky wave applications.

C. Effect of a backplane

We now consider the effect of a perfect electric conductor backplane placed a distance h away from the graphene microribbon on the substrate side. There are two possible motivations for this: radiation control, and electrostatic gating. We simulate several different backplane distances h using Design A and obtain their corresponding dispersion relationships. First, we consider $h = 8$ μm which corresponds to approximately $\lambda/4$ at 2.8 THz within silicon. At this distance the ground plane is sufficiently far away such that there is little interaction between it and the fringing fields of the graphene plasmonic mode; the dispersion relation is unaffected (see Fig. 8). The radiative quality factor is also similar in magnitude to the case without the backplane. However, care must be taken when adding a backplane when the dielectric thickness is close to a quarter wavelength, as undesirable

coupling with surface waves may result.[44] A straightforward solution to suppress these parasitic modes is to etch the dielectric slab into a ridge underneath the graphene. Such a structure will prevent excitation of surface waves, while leaving the near-field and dispersion relation unchanged. Although not shown here, simulations show that this scheme preserves the scanning beam behavior except into the air side rather than the substrate.

A smaller backplane separation can be used to reduce radiative loss as well as allow for electrostatic gating of the graphene. As seen in Fig. 8 the presence of the backplane significantly changes the dispersion relation for $h = 1$ μm as ω_{sh} drops due to the increase in shunt capacitance C_R that results from interaction with the ground plane. For the case of $h = 0.2$ μm the change is so large that a redesign is necessary to "re-balance" the CRLH waveguide; the dimensions and dispersion is shown in Fig. 8 for this "Design A′". The width was reduced to 1.9 μm to increase ω_{sh} back to 2.8 THz. However, since the reduction in w also reduces C_L, the gap a is reduced to 25 nm to keep ω_{se} constant. The presence of such a close backplane effectively shorts out the radiation of the CRLH structure via the image currents, and the radiative quality factor becomes very large ($Q_r \gg 10^4$). This configuration will also allow tuning of the CRLH dispersion via backgating of the carrier density with modest voltages, perhaps for applications such as phase shifters or tunable resonators. Comparison with recent experimental results with similar gate dielectric thicknesses (in SiO_2) suggests that voltages on the order of 50–100 V would be required to tune the Fermi level from the Dirac point to the values of 0.5-1 eV necessary for our designs.[12,45] An alternative to reduce the gate voltage and obviate the need for a backgate is to use an ion-gel top-gate, which has been shown to modulate the Fermi level over 1 eV with a voltage swing of < 10 V.[45]

V. CONCLUSION

In this work we have introduced a new design paradigm for graphene plasmonic CRLH waveguides and presented several designs in the terahertz frequency range. We have also characterized free-carrier and radiative losses, leaky-wave antenna radiation patterns, and the effects of carrier density tuning. A transmission-line model provides qualitative design guidance, and quantitative agreement with numerical results with the assistance of fitting parameters. The dimensional requirements are challenging (i.e. the 2.8 THz design has ribbons of width 4.5 μm and gaps of 100 nm, the 12 THz design has ribbons of width 260 nm

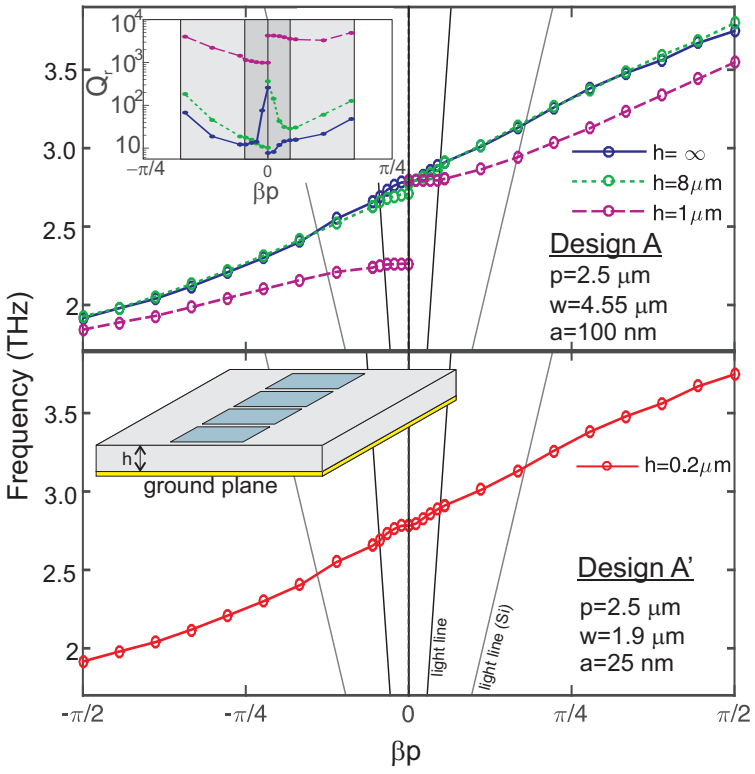

FIG. 8. Dispersion relationship and associated radiative quality factor Q_r (inset) for Design A with an infinite groundplane distance h placed below the graphene strips. When the groundplane is placed close at $h = 0.2$ μm, Design A must be rebalanced; this new design is labeled Design A$'$.

and gaps of 19 nm), but within what is achievable using electron-beam lithography. However, the primary challenges for scaling to higher frequencies is the requirement that dimensions shrink quadraditically with frequency as dictated by the square root dispersion relation. The gap size a is the smallest critical dimension, and will likely be the primary limiting factor for fabrication if these structures were to be scaled up to the mid-IR, since it would need to shrink to just a few nanometers.

The issue of loss is the most critical challenge for practical CRLH graphene devices. For example at 3 THz, for practical values of the graphene mobility (i.e. τ=1 ps, $\mu \approx 15,600\,\mathrm{cm}^2/\mathrm{V}\cdot\mathrm{s}$), losses are large and propagation lengths limited. Radiative losses are also large – this benefits radiative efficiency for leaky-wave antennas, but results in reduced beam scanning and large beamwidths. Hence, the most critical challenge for practical implementation is the need for large-area high-mobility graphene to minimize plasmon dissipation and achieve times of $\tau > 1$ ps. For guided wave operation, radiative losses can be eliminated

with the addition of a backplane, which can also act as a backgate for free-carrier tuning. By tuning the carrier concentration by one order of magnitude, 180 degrees of phase shift can be obtained even over the length of one unit cell – an attractive feature for a distributed phase shifter. The situation for losses improves somewhat at higher frequencies (i.e. 5 THz and 12 THz), since the Drude quality factor for CRLH modes scales proportionally to ω, and the radiative quality factor Q_r scales as ω^2 due to the quadratic reduction in waveguide dimensions. These challenges are not unique to our design – indeed they are ubiquitous for any device based upon plasmons.[46] However, the reduced group velocity of the CRLH waveguide reduces the propagation length by a factor two and the Q by a factor of $\sim$0.75 compared to an unpatterned graphene plasmon.

In summary, our results show that while demonstrating CRLH graphene waveguides is possible, it will be challenging, with the ultimate performance highly dependent upon availability of high-mobility graphene with long Drude relaxation times. This challenge will need to be weighed against potential benefits of using graphene, such as free-carrier tunability, or large optical nonlinearity.

ACKNOWLEDGMENTS

The authors would like to thank Ziwen Wang for his preliminary simulation work. This research was supported in part by National Science Foundation grants ECCS 1150071 and ECCS 1340928.

Appendix: CRLH Transmission Line Model

The theory of CRLH metamaterials is most easily presented in terms of a transmission-line model. In the graphene microribbon waveguide presented here, this is not strictly valid since the CRLH behavior is based upon a higher-order transverse mode, which results in an approximately sinusoidal variation in the electric and magnetic fields across the width of the ribbon. Thus, the waveguide cannot be considered sub-wavelength in the transverse dimension, and the quasi-static limit is not applicable. Nonetheless, a circuit model is still very useful for qualitative understanding and design guidance, *provided that it is understood that inductances and capacitances are effective parameters.* However for detailed design

numerical methods must be used. We begin by defining the series inductance L_R and shunt capacitance C_R for a graphene microribbon with an effective width w_{eff} and unit cell length p:

$$L_R = -\frac{p}{w_{\text{eff}}\omega}\text{Im}\{\sigma^{-1}\} = \frac{p\pi\hbar^2}{w_{\text{eff}}e^2E_F} \tag{A.1}$$

$$C_R = D_R p w_{\text{eff}}\left(\varepsilon_1+\varepsilon_2\right)\text{Re}\{q(\omega)\} \tag{A.2}$$

$$= D_R\frac{p w_{\text{eff}}\pi\hbar^2\left(\varepsilon_1+\varepsilon_2\right)^2}{e^2E_F}\omega^2 \tag{A.3}$$

The series inductance L_R originates from the kinetic inductance of the graphene free carriers, i.e. the imaginary part of the Drude resistivity in (2). We neglect any additional "Faraday inductance" associated with the graphene currents, which is negligible in the non-retarded limit (i.e. $q \gg \omega/c$).[31] The effective shunt capacitance C_R was obtained by equating the dispersion relation of a conventional transmission line $\beta = \omega\frac{\sqrt{L_RC_R}}{p}$ to the graphene plasmon dispersion relation given in (4) for an infinite graphene sheet. This requires C_R to acquire a frequency/wavenumber dependence. However, an additional factor D_R has been added which enhances the capacitance to account for the modification of the dispersion due to the finite width of the microribbon. D_R can be obtained either through matching to numerical simulations, or by using the term η calculated in Ref. 34 ($D_R \approx (2\pi^2\eta)^2$ in which η is evaluated at $qw = \pi$). Using this expression, we accordingly take D_R=1.8, 1.8, and 1.9 for Designs A, B, and C respectively. This expression for C_R also neglects the effects of quantum-capacitance, which is appropriate here where the non-local corrections to conductivity are negligible.[30,31] For the fundamental lateral mode $m = 0$, the effective width w_{eff} is equal to the physical ribbon width w. In this case, these expressions are equivalent to those derived in Ref. 31, taken in the limit that $k_BT \ll E_F$, and ignoring the negligible contributions of quantum capacitance, and Faraday inductance.

The CRLH waveguide mode is based upon an $m = 1$ higher order lateral mode (i.e. an edge mode), and includes series capacitive gaps of size a. We model this according to the double transmission line circuit model shown in Fig. 2(d) operating in its odd mode. The previous expressions for L_R and C_R still apply, provided that the effective width in this case is $w_{\text{eff}} = Fw/2$. This reflects the fact that branch of the TL has physical width of $w/2$, and the effective width is modified by a factor F to reflect that the current, field, and charge are nonuniform over the width of the ribbon. We can approximate this factor as $F = 2/\pi A$; ideally $A = 1$, which is appropriate for a field distribution takes on exactly a half-sinusoidal

transverse variation.[27] In reality, there is a slight phase shift associated with the reflection of the plasmon from the microribbon edge; we find A=0.9, 0.96, and 1.0 for designs A, B, and C respectively. We also define the shunt inductance:

$$L_L = -\frac{w_{\text{eff}}}{p\omega}\text{Im}\{\sigma^{-1}\} = \frac{w_{\text{eff}}\pi\hbar^2}{pe^2E_F}, \tag{A.4}$$

which is based upon the same kinetic inductance of the graphene used to define L_R, except now for a section of length of w_{eff} and width of p. This ensures that the effective shunt frequency $\omega_{sh} = (L_L C_R)^{-1/2}$ corresponds the condition where the microribbon width w is nearly equal to one-half of the plasmon wavelength such that $q(\omega_{sh}) = A\pi/w$.

A working expression for the series capacitance C_L can be obtained from the capacitance between metal patches of width w_{eff} and length $p/2$ on a dielectric half-space in the limit that $p \gg a$ (derived for a Sievenpiper surface in Ref. 47), which gives

$$C_L = D_L\frac{w_{\text{eff}}}{\pi}\left(\varepsilon_1 + \varepsilon_2\right)\ln\left(2p/a\right). \tag{A.5}$$

D_L is a phenomenological factor that is required to reduce $\omega_{se} = (L_R C_L)^{-1/2}$ so that it matches the simulated result. We fit the values of D_L=0.7, 0.66, and 0.6 for the dimensions of designs A, B, and C respectively. Without this factor, C_L is overestimated since the period of the structure is not sufficiently subwavelength to accurately use a lumped element expression.

Despite the presence of the phenomenological parameters, we can still draw important conclusions. For example, by equating these analytic expressions for the series and shunt resonance frequencies, we are able to obtain a transcendental equation for the CRLH balanced condition:

$$D_L\ln(2p/a) = \frac{w}{p}\frac{\sqrt{D_R}}{A}. \tag{A.6}$$

This expression for the balanced condition contains only geometric parameters; there is no dependence on carrier concentration or other material properties. This implies that the balanced dispersion relation will be preserved as the carrier density is changed, which is consistent with the tuning observed in the numerical simulations in Fig. 4.

Drude loss within the graphene can be included by adding resistances

$$R_R = \frac{2p\pi\hbar^2}{w_{\text{eff}}e^2E_F\tau}, R_L = \frac{2w_{\text{eff}}\pi\hbar^2}{pe^2E_F\tau} \tag{A.7}$$

in series with L_R and L_L respectively. We can further use this formalism to derive an analytic expression for loss in a CRLH waveguide. The dispersion for a balanced line is given:[25]

$$\beta = \frac{\omega}{p}\sqrt{(L_R + iR_R/\omega)\,C_R} - \frac{1}{p\omega}\frac{1}{\sqrt{(L_L + iR_L/\omega)\,C_L}}. \tag{A.8}$$

This gives a power attenuation coefficient

$$\alpha = 2\mathrm{Im}\{\beta\} = \frac{2}{p\tau}\sqrt{L_R C_R} + \frac{2}{p\omega^2\tau}\frac{1}{\sqrt{L_L C_L}}. \tag{A.9}$$

For a balanced CRLH structure, at $\beta = 0$, the attenuation coefficient is:

$$\alpha(\omega = \omega_{sh} = \omega_{se}) = \frac{4}{p\tau}\sqrt{L_R C_R} = \frac{4\pi\hbar^2\,(\varepsilon_1 + \varepsilon_2)\,\omega}{\tau e^2 E_F}, \tag{A.10}$$

which is twice as large as for an unpatterned $m = 0$ graphene plasmon mode at the same frequency. The quality factor associated with Drude loss can then be obtained using the relation $Q_D = \omega/\alpha v_g$; at $\beta = 0$ it has the value of

$$Q_D = \omega/\alpha v_g, \tag{A.11}$$

This relation is used to estimate the Drude losses in Fig. 6. We note that at $\beta = 0$, $Q_D = (3/4)\omega\tau$ – three quarters of the value of Q_D of an unpatterned $m = 0$ graphene plasmon.

REFERENCES

[1] M. Jablan, H. Buljan, and M. Soljačić, "Plasmonics in graphene at infrared frequencies," Phys. Rev. B **80**, 245435 (2009).

[2] E. H. Hwang and S. Das Sarma, "Dielectric function, screening, and plasmons in two-dimensional graphene," Phys. Rev. B **75**, 205418 (2007).

[3] F. H. L. Koppens, D. E. Chang, and F. J. García de Abajo, "Graphene plasmonics: A platform for strong light matter interactions," Nano Lett. **11**, 3370–3377 (2011).

[4] A. Y. Nikitin, F. Guinea, F. J. García-Vidal, and L. Martín-Moreno, "Edge and waveguide terahertz surface plasmon modes in graphene microribbons," Phys. Rev. B **84**, 161407 (2011).

[5] A. N. Grigorenko, M. Polini, and K. S. Novoselov, "Graphene plasmonics," Nature Photon. **6**, 749–758 (2012).

[6]Z. Fei, G. O. Andreev, W. Bao, L. M. Zhang, A. S. McLeod, C. Wang, M. K. Stewart, Z. Zhao, G. Dominguez, M. Thiemens, M. M. Fogler, M. J. Tauber, A. H. Castro-Neto, C. N. Lau, F. Keilmann, and D. N. Basov, "Infrared nanoscopy of dirac plasmons at the graphene-SiO_2 interface," Nano Lett. **11**, 4701–4705 (2011).

[7]Z. Fei, A. S. Rodin, G. O. Andreev, W. Bao, A. S. McLeod, M. Wagner, L. M. Zhang, Z. Zhao, M. Thiemens, G. Dominguez, M. M. Fogler, A. H. C. Neto, C. N. Lau, F. Keilmann, and D. N. Basov, "Gate-tuning of graphene plasmons revealed by infrared nano-imaging," Nature (2012), 10.1038/nature11253.

[8]A. Woessner, M. B. Lundeberg, Y. Gao, A. Principi, P. Alonso-González, M. Carrega, K. Watanabe, T. Taniguchi, G. Vignale, M. Polini, J. Hone, R. Hillenbrand, and F. H. L. Koppens, "Highly confined low-loss plasmons in graphene-boron nitride heterostructures," Nature Mater. **14**, 421–425 (2014).

[9]J. Chen, M. Badioli, P. Alonso-González, S. Thongrattanasiri, F. Huth, J. Osmond, M. Spasenović, A. Centeno, A. Pesquera, P. Godignon, A. Z. Elorza, N. Camara, F. J. G. de Abajo, R. Hillenbrand, and F. H. L. Koppens, "Optical nano-imaging of gate-tunable graphene plasmons," Nature (2012), 10.1038/nature11254.

[10]L. Ju, B. Geng, J. Horng, C. Girit, M. Martin, Z. Hao, H. A. Bechtel, X. Liang, A. Zettl, Y. R. Shen, and F. Wang, "Graphene plasmonics for tunable terahertz metamaterials," Nature Nanotech. **6**, 630–634 (2011).

[11]H. Yan, X. Li, B. Chandra, G. Tulevski, Y. Wu, M. Freitag, W. Zhu, P. Avouris, and F. Xia, "Tunable infrared plasmonic devices using graphene/insulator stacks," Nature Nanotech. **7**, 330–334 (2012).

[12]V. W. Brar, M. S. Jang, M. Sherrott, J. J. Lopez, and H. A. Atwater, "Highly confined tunable mid-infrared plasmonics in graphene nanoresonators," Nano Lett. **13**, 2541–2547 (2013).

[13]H. Yan, T. Low, W. Zhu, Y. Wu, M. Freitag, X. Li, F. Guinea, P. Avouris, and F. Xia, "Damping pathways of mid-infrared plasmons in graphene nanostructures," Nature Photon. **7**, 394–399 (2013).

[14]X. Zhu, W. Wang, W. Yan, M. B. Larsen, P. Bøggild, T. G. Pedersen, S. Xiao, J. Zi, and N. A. Mortensen, "Plasmon-phonon coupling in large-area graphene dot and antidot arrays fabricated by nanosphere lithography," Nano Lett. **14**, 2907–2913 (2014).

[15]R. Yan, B. Sensale-Rodriguez, L. Liu, D. Jena, and H. G. Xing, "A new class of electrically

tunable metamaterial terahertz modulators," Opt. Express **20**, 28664 (2012).

[16]B. Sensale-Rodriguez, R. Yan, M. M. Kelly, T. Fang, K. Tahy, W. S. Hwang, D. Jena, L. Liu, and H. G. Xing, "Broadband graphene terahertz modulators enabled by intraband transitions," Nature Commun. **3**, 780 (2012).

[17]S. H. Lee, M. Choi, T.-T. Kim, S. Lee, M. Liu, X. Yin, H. K. Choi, S. S. Lee, C.-G. Choi, S.-Y. Choi, X. Zhang, and B. Min, "Switching terahertz waves with gate-controlled active graphene metamaterials," Nature Mater. **11**, 936–941 (2012).

[18]M. Esquius-Morote, J. S. Gómez-Díaz, and J. Perruisseau-Carrier, "Sinusoidally modulated graphene leaky-wave antenna for electronic beamscanning at THz," IEEE Trans. THz Sci. Tech. **4**, 116–122 (2014).

[19]R. Filter, M. Farhat, M. Steglich, R. Alaee, C. Rockstuhl, and F. Lederer, "Tunable graphene antennas for selective enhancement of THz-emission," Opt. Express **21**, 3737–3745 (2013).

[20]I. Llatser, C. Kremers, A. Cabellos-Aparicio, E. A. Josep Miquel Jornet, and D. N. Chigrin, "Graphene-based nano-patch antenna for terahertz radiation," Photonics and Nanostructures - Fundamentals and Applications **10**, 353–358 (2012).

[21]J. S. Gómez-Díaz, M. Esquius-Morote, and J. Perruisseau-Carrier, "Plane wave excitation-detection of non-resonant plasmons along finite-width graphene strips," Opt. Express **21**, 24856–24872 (2013).

[22]C. Caloz and T. Itoh, "Application of the transmission line theory of left-handed (LH) materials to the realization of a microstrip LH transmission line," Proc. IEEE-AP-S USNC/URSI National Radio Science Meeting **2**, 412–415 (2002).

[23]A. Lai, C. Caloz, and T. Itoh, "Composite right/left handed transmission line metamaterials," IEEE Microwave Magazine **5**, 34–50 (2004).

[24]G. V. Eleftheriades, A. K. Iyer, and P. C. Kremer, "Planar negative refractive index media using periodically L-C loaded transmission lines," IEEE Trans. Microw. Theory Tech. **50**, 2702–2712 (2002).

[25]C. Caloz and T. Itoh., *Electromagnetic Metamaterials: Transmission Line Theory and Microwave Applications* (Wiley, 2006).

[26]A. A. Tavallaee, P. W. C. Hon, Q.-S. Chen, T. Itoh, and B. S. Williams, "Active terahertz quantum-cascade composite right/left-handed metamaterial," Appl. Phys. Lett. **102**, 021103 (2013).

[27]P. W. C. Hon, Z. Liu, T. Itoh, and B. S. Williams, "Leaky and bound modes in terahertz metasurfaces made of transmission-line metamaterials," J. Appl. Phys. **113**, 033105 (2013).

[28]J. Horng, C.-F. Chen, B. Geng, C. Girit, Y. Zhang, Z. Hao, H. Bechtel, M. Martin, A. Zettl, M. Crommie, Y. Shen, and F. Wang, "Drude conductivity of dirac fermions in graphene," Phys. Rev. B **83**, 165113 (2011).

[29]F. J. García de Abajo, "Graphene plasmonics: Challenges and opportunities," ACS Photonics **1**, 135–152 (2014).

[30]G. Lovat, G. W. Hanson, R. Araneo, and P. Burghignoli, "Semiclassical spatially dispersive intraband conductivity tensor and quantum capacitance of graphene," Phys. Rev. B **87**, 115429 (2013).

[31]D. Correas-Serrano, J. S. Gómez-Díaz, J. Perruisseau-Carrier, and A. Álvarez Melcón, "Spatially dispersive graphene single and parallel plate waveguides: analysis and circuit model," IEEE Trans. THz Sci. Tech. **61**, 4333–4343 (2013).

[32]S. Thongrattanasiri, A. Manjavacas, and F. J. García de Abajo, "Quantum finite-size effects in graphene plasmons," ACS Nano **6**, 1766–1775 (2012).

[33]A. Fallahi, T. Low, M. Tamagnone, and J. Perruisseau-Carrier, "Nonlocal electromagnetic response of graphene nanostructures," Phys. Rev. B **91**, 121405(R) (2015).

[34]J. Christensen, A. Manjavacas, S. Thongrattanasiri, F. H. L. Koppens, and F. J. García de Abajo, "Graphene plasmon waveguiding and hybridization in individual and paired nanoribbons," ACS Nano **6**, 431–440 (2012).

[35]A. A. Tavallaee, B. S. Williams, P. W. C. Hon, T. Itoh, and Q.-S. Chen, "Terahertz quantum-cascade laser with active leaky-wave antenna," Appl. Phys. Lett. **99**, 141115 (2011).

[36]J. Gomez-Diaz and J. Perruisseau-Carrier, "Microwave to THz properties of graphene and potential antenna applications," in *Antennas and Propagation (ISAP), 2012 International Symposium on* (2012) pp. 239–242.

[37]J. S. Gómez-Díaz, D. Canete-Rebenaque, and A. Álvarez Melcón, "A simple CRLH LWA circuit condition for constant radiation rate," IEEE Antennas and Wireless Propag. Lett. **10**, 29–32 (2011).

[38]S. Otto, A. Rennings, K. Solbach, and C. Caloz, "Transmission line modeling and asymptotic formulas for periodic leaky-wave antennas scanning through broadside," IEEE Trans. Antennas Propag. **59**, 3695–3709 (2011).

[39]K. I. Bolotin, K. J. Sikes, Z. Jiang, M. Klima, G. Fudenberg, J. Hone, P. Kim, and H. L. Stormer, "Ultrahigh electron mobility in suspended graphene," Solid State Commun. **146**, 351–355 (2008).

[40]W. Gannett, W. Regan, K. Watanabe, T. Taniguchi, M. F. Crommie, and A. Zettl, "Boron nitride substrates for high mobility chemical vapor deposited graphene," Appl. Phys. Lett. **98**, 242105 (2011).

[41]C. R. Dean, A. F. Young, I. Meric, C. Lee, L. Wang, S. Sorgenfrei, K. Watanabe, T. Taniguchi, P. Kim, K. L. Shepard, and J. Hone, "Boron nitride substrates for high-quality graphene electronics," Nature Nanotech **5**, 722–726 (2010).

[42]S. Lim, C. Caloz, and T. Itoh, "Metamaterial-based electronically controlled transmission-line structure as a novel leaky-wave antenna with tunable radiation angle and beamwidth," IEEE Trans. Microw. Theory Tech. **53**, 161–173 (2005).

[43]E. R. Brown, K. A. McIntosh, K. B. Nichols, and C. L. Dennis, "Photomixing up to 3.8 THz in low-temperature-grown GaAs," Appl. Phys. Lett. **66**, 285–287 (1995).

[44]A. Shahvarpour, A. Álvarez Melcón, and C. Caloz, "Radiation efficiency issues in planar antennas on electrically thick substrates and solutions," IEEE Trans. Antennas Propag. **61**, 4013–4025 (2013).

[45]H. Hu, F. Zhai, D. Hu, Z. Li, B. Bai, X. Yang, and Q. Dai, "Broadly tunable graphene plasmons using an ion-gel top gate with low control voltage," Nanoscale **7**, 19493–19500 (2015).

[46]J. B. Khurgin, "How to deal with the loss in plasmonics and metamaterials," Nature Nanotech. **10**, 2–6 (2015).

[47]D. F. Sievenpiper, *High-Impedance Electromagnetic Surfaces*, Ph.D. thesis (1999).